Geochemical Perspectives Letters

Diffusional fractionation of neon isotopes in MORB melts: a molecular dynamics study

J. Nteme[1*], M. Moreira[1]

OPEN ACCESS

https://doi.org/10.7185/geochemlet.2630

Abstract

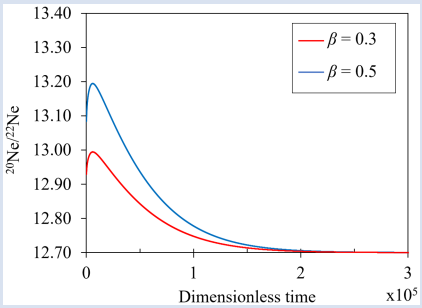

Neon isotopes are key tracers of Earth's volatile origin, yet their signatures in volcanic glasses may be modified by kinetic fractionation during magmatic degassing. Recent experiments have revealed vesicle-scale variations in $^{20}Ne/^{22}Ne$, highlighting the need for quantitative constraints on the mass dependence of neon diffusion in silicate melts. Here, we use classical molecular dynamics simulations and a pseudo-isotope approach to determine the mass dependence exponent β for neon diffusion in a MORB melt over temperatures of 1473–1873 K and pressures of 0 to 10 kbar. We find a robust linear relationship between log D and log m, with $\beta \approx 0.24$–0.29 at low pressure, significantly lower than the gas kinetic prediction of 0.5, and decreasing approximately linearly with pressure. These results indicate that diffusion-driven fractionation is limited at the melt scale but can generate measurable, transient isotopic enrichments in vesicles under strongly non-equilibrium degassing conditions. Our findings provide a physically grounded framework for interpreting neon isotope signatures in MORB glasses and assessing the preservation of mantle-derived volatile signals.

Received 25 March 2026 | Accepted 16 July 2026 | Published 7 September 2026

Introduction

The origin and evolution of highly volatile elements on Earth remain central questions in planetary science. These elements originate from multiple sources in the early Solar System and their present-day signatures reflect a complex history of planetary accretion, differentiation, degassing and loss to space (Marty *et al.*, 2016; Avice *et al.*, 2017; Bekaert *et al.*, 2019; Péron *et al.*, 2018, 2021). Noble gases are particularly valuable tracers of these processes because of their chemical inertness: their isotopic compositions are unaffected by biological or chemical reactions and are modified only by physical mechanisms such as diffusion, adsorption, or ion implantation (Ozima and Podosek, 1983; Moreira, 2013). Among them, neon provides a unique window into Earth's volatile history, as its two primordial isotopes (^{20}Ne and ^{22}Ne) are negligibly produced by nuclear reactions in the mantle (Yatsevich and Honda, 1997) and thus potentially record the incorporation of a primordial component during Earth's formation (Sarda *et al.*, 1988; Honda *et al.*, 1993; Moreira *et al.*, 1995, 1998). It is now well established that the mantle $^{20}Ne/^{22}Ne$ ratio is solar-like, although its exact value and spatial homogeneity within the mantle remain debated (Sarda *et al.*, 1988; Honda *et al.*, 1993; Moreira *et al.*, 1995, 1998, 2001; Trieloff *et al.*, 2002; Ballentine *et al.*, 2005; Kurz *et al.*, 2009). Competing models attribute mantle neon either to the dissolution of a solar-captured proto-atmosphere into a global magma ocean (*e.g.*, Mizuno *et al.*, 1980), or to the accretion of solar-wind-irradiated dust into Earth's parent bodies (Ballentine *et al.*, 2005; Kurz *et al.*, 2009; Moreira and Charnoz, 2016; Péron *et al.*, 2016, 2017, 2018).

Distinguishing between these scenarios requires understanding how neon isotopes fractionate during magmatic processes. Volcanic glasses from mid-ocean ridge basalts (MORBs) and ocean island basalts (OIBs) provide access to the mantle neon signature. However, their interpretation is complicated by possible isotopic fractionation during magma ascent and degassing. Degassing of basaltic melts is primarily driven by CO_2 exsolution, leading to bubble nucleation and growth. Because Ne is highly incompatible in silicate melts, it partitions strongly into vesicles, where isotopic fractionation may occur if diffusion rates differ between isotopes. Lighter ^{20}Ne atoms are expected to diffuse faster than ^{22}Ne, potentially enriching early-formed vesicles in ^{20}Ne relative to the residual melt. This kinetic isotope effect could alter the isotopic ratios measured in natural samples and bias estimates of the mantle source composition. Until recently, direct evidence for such fractionation was lacking. Laboratory experiments by Núñez-Guerrero *et al.* (2025) demonstrated for the first time that individual vesicles in vesiculated basaltic glasses exhibit measurable variations in $^{20}Ne/^{22}Ne$, consistent with kinetic mass-dependent fractionation during disequilibrium degassing. These results highlight the importance of diffusion-driven fractionation in natural magmatic systems and underscore the need for quantitative models capable of predicting its magnitude under mantle conditions.

A key parameter characterising isotope-dependent diffusion is the mass dependence exponent β, defined through the relation:

$$\frac{D_i}{D_j} = \left(\frac{m_j}{m_i}\right)^{\beta} \qquad \text{(Eq. 1)}$$

1. Univ. Orléans, CNRS, BRGM, Institut des Sciences de la Terre d'Orléans (ISTO), UMR 7327, F-45071, Orléans, France
* Corresponding author (email: jehiel.nteme-mukonzo@univ-orleans.fr)

where D_i and D_j are the diffusion coefficients of isotopes with masses m_i and m_j, respectively. In noble gas isotope fractionation studies, $\beta = 0.5$ is often adopted when isotope-specific diffusion data are unavailable. This assumption originates from Graham's law of diffusion and effusion in gases (Graham, 1833), which predicts that the transport rate of a particle is inversely proportional to the square root of its mass. While Graham's law applies to free particles in the gas phase, atomistic interactions in dense silicate melts are expected to reduce the influence of mass on diffusivity. For helium, recent molecular dynamics studies using advanced neural network potentials showed that β indeed departs significantly from 0.5, taking values of 0.27–0.36 depending on melt composition and temperature (Luo *et al.*, 2021a). However, no equivalent quantitative constraints exist for neon, despite its critical role as a tracer of mantle processes.

In this study, we address this gap by performing classical molecular dynamics simulations of neon diffusion in a representative MORB melt. Using the pseudo-isotope method, which artificially extends the mass range beyond natural isotopes while preserving interatomic interactions, we systematically quantify the dependence of diffusion on mass across temperatures from 1473 K to 1873 K and pressures of 0, 5, and 10 kbar. From these simulations, we derive robust β values for neon in silicate melts, evaluate their dependence on temperature and pressure, and assess their implications for isotope fractionation during magma degassing. Our results provide a quantitative framework for interpreting experimental observations of neon isotopic variations in vesicles, refining models of noble gas loss during magmatic ascent, and constraining the preservation of primitive volatile signatures in Earth's mantle.

Methods

Molecular dynamics (MD) simulations were performed using the LAMMPS package (Thompson *et al.*, 2022). The simulated system consisted of 3,000 melt atoms and a single Ne atom in a cubic simulation cell with periodic boundary conditions. The melt structure was described using an empirical potential developed for silicate melts of the KNCFMATS system (K_2O-Na_2O-CaO-FeO-MgO-Al_2O_3-TiO_2-SiO_2), which has been shown to accurately reproduce key thermodynamic and transport properties of these melts (Guillot and Sator, 2007). The melt composition and all interaction parameters are reported in Tables S-1 to S-3.

The initial melt configuration was generated by randomly distributing the melt-forming atoms within the simulation cell. The system was first equilibrated at 4000 K and 10 kbar to remove any structural bias associated with the initial random configuration. A single Ne atom was subsequently introduced into the equilibrated melt, and the system was equilibrated for an additional 1 ns at each target temperature and pressure. Production runs were then carried out for 10 ns in the NVT ensemble using a Nosé-Hoover thermostat with a timestep of 1 fs. Long-range electrostatic interactions were evaluated using the particle-particle particle-mesh (PPPM) method, while short-range interactions were truncated at 10 Å.

The mass dependence of diffusion was investigated using the pseudo-isotope approach (*e.g.*, Goel *et al.*, 2012; Luo *et al.*, 2020, 2021a, 2021b), in which artificial isotopes with modified masses but identical interaction parameters are introduced to amplify kinetic isotope effects. In addition to natural ^{20}Ne, pseudo-masses of 4, 8, 12, and 16 g/mol were simulated. Diffusion coefficients were determined from the linear regime of the mean squared displacement (MSD) using the Einstein relation:

$$D = \lim_{t\to\infty} \frac{\langle \Delta r(t)^2 \rangle}{6t} \qquad \text{(Eq. 2)}$$

where $\langle \Delta r(t)^2 \rangle$ is the ensemble-averaged MSD. For each mass-temperature-pressure condition, 20 independent simulations were performed, and MSDs were averaged over multiple time origins using 100 segments of 100 ps. Final diffusion coefficients are reported as the mean across all runs, with uncertainties given as the standard error of the mean. The mass dependence exponent β was obtained from linear regressions of log D *versus* log m.

Results

To evaluate the influence of isotopic mass on diffusion, we first verified that the diffusion process was properly sampled in our simulations. Figure 1a shows the MSD of Ne atoms at different temperatures under near-zero-pressure conditions. The MSD curves exhibit the expected two-stage behaviour: an initial ballistic regime lasting about 1 ps, followed by diffusive behaviour at longer times. MSD curves for different pseudo-isotopes are clearly separated. Diffusion coefficients derived from the MSD curves are reported in Table S-4. They follow the expected

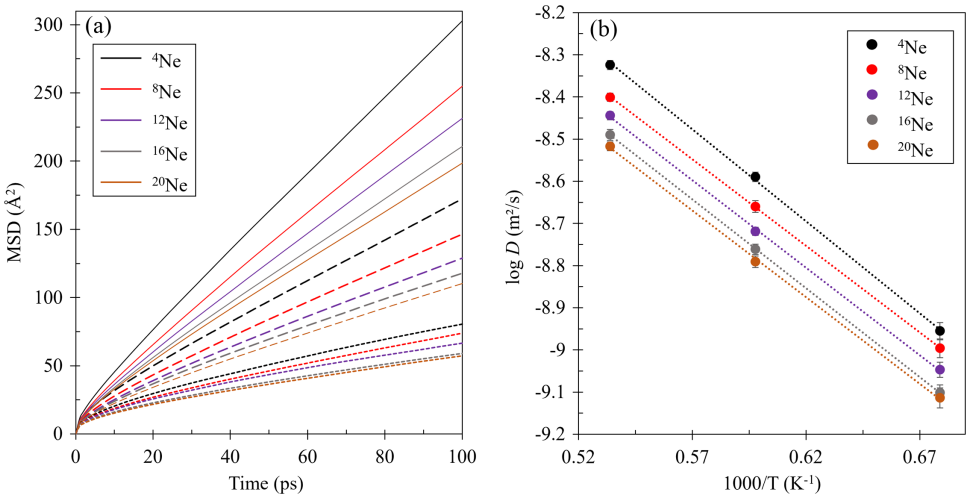

Figure 1 **(a)** Mean squared displacement (MSD) of Ne pseudo-isotopes in MORB melt at near-zero pressure and temperatures of 1473 K (dotted), 1673 K (dashed), and 1873 K (solid). **(b)** Diffusion coefficients as a function of inverse temperature.

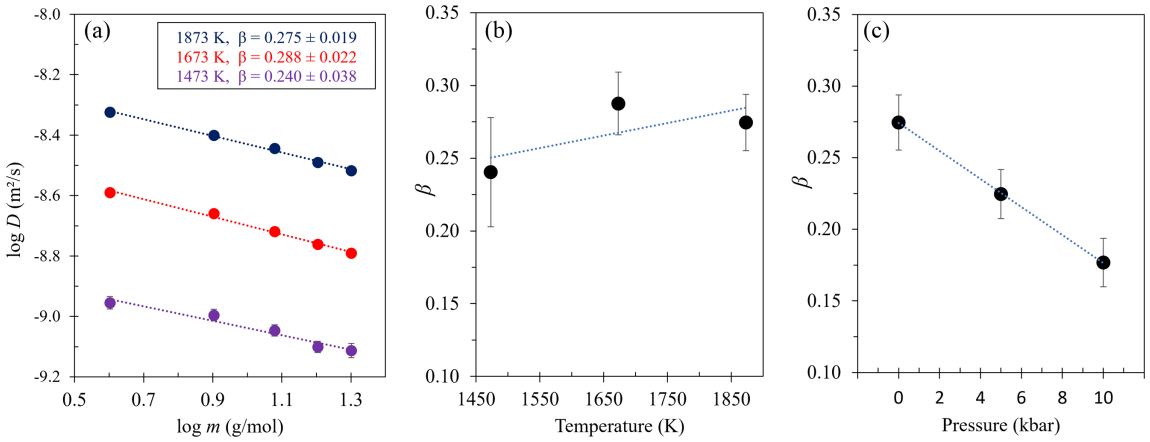

Figure 2 **(a)** Log D versus log m for Ne pseudo-isotopes at different temperatures. **(b)** Mass dependence exponent β as a function of temperature. **(c)** β as a function of pressure at 1873 K.

trends: diffusivity decreases with increasing isotopic mass, increases with temperature, and decreases with pressure. The temperature dependence follows an Arrhenius law:

$$D(T) = D_0 \exp\left(-\frac{E_a}{RT}\right), \qquad \text{(Eq. 3)}$$

where D_0 is the pre-exponential factor, E_a is the activation energy and R is the gas constant. This relationship holds for all neon isotopes investigated (Fig. 1b). The calculated D_0 values appear to decrease with increasing mass, whereas the activation energies show no definite mass dependence and remain within the range 78–83 kJ/mol (Fig. S-1). The predicted diffusivity for ^{20}Ne at 1623 K is 1.38×10^{-9} m^2/s, which is of the same order of magnitude as the experimental value of 2.75×10^{-9} m^2/s reported by Lux (1987).

The dependence of diffusion on isotopic mass is well captured by the linear relationship between log D and log m across the entire temperature range investigated (Fig. 2a). This demonstrates that isotopic mass influences neon mobility in MORB melts at zero pressure. From these regressions, we derive the mass dependence exponent β. Unlike the gas kinetic prediction of β = 0.5, our values are significantly lower, ranging from 0.240 ± 0.038 at 1473 K to 0.288 ± 0.022 at 1673 K and 0.275 ± 0.019 at 1873 K. This reduction reflects the influence of the dense silicate network, which hinders isotopic separation compared to gaseous systems. The β *versus* temperature relationship (Fig. 2b) suggests a weak positive correlation, corresponding to slightly higher β values at elevated temperatures. However, this trend remains within analytical uncertainty and does not support a statistically significant temperature dependence of β over the investigated range. This contrasts with previous studies reporting a decrease of β with increasing temperature in silicate melts at near-zero pressure for lighter species such as He and Li (*e.g.*, Luo *et al.*, 2021a, 2021b).

At elevated pressures, the linear relationship between log D and log m is preserved at 1873 K (Fig. S-3), indicating that isotopic mass still exerts an influence on neon diffusion. β decreases approximately linearly with pressure, varying from 0.275 at ambient pressure to 0.225 ± 0.017 at 5 kbar and 0.177 ± 0.017 at 10 kbar (Fig. 2c). This behaviour is consistent with observations for Mg diffusion in silicate melts, where the mass dependence weakens with increasing pressure (*e.g.*, Goel *et al.*, 2012; Luo *et al.*, 2020). In those systems, the reduction in β has been attributed to pressure-induced structural compaction, which increases atomic coordination and reduces the free volume available for uncorrelated motion. Although neon is an inert, non-bonding species, a similar effect may operate indirectly, as increased network rigidity constrains transport pathways and promotes more collective motion, thereby attenuating the isotopic mass effect.

Previous studies have proposed that β in silicate melts increases with the solvent-normalised diffusivity (D_i/D_{Si}), suggesting that species weakly coupled to the silicate network tend to exhibit stronger isotopic fractionation during diffusion (*e.g.*, Watkins *et al.*, 2011). However, Luo *et al.* (2020, 2021a) argued that this relationship is valid only over a limited temperature range and becomes less systematic when comparing different elements and melt compositions. Our results support this more nuanced interpretation. Although D_{Ne}/D_{Si} is substantially lower than D_{He}/D_{Si} in basaltic melts at comparable temperatures (~1700 K; Luo *et al.*, 2021a), Ne exhibits a β value (0.288 ± 0.022) very similar to that of He (Fig. 3). If β were controlled solely by D_i/D_{Si}, a much larger difference between He and Ne would be expected. Instead, the similarity of their β values suggests that the mass dependence of diffusion for small noble gases is affected by the silicate network in a comparable manner, despite significant differences in their absolute diffusivities.

This behaviour likely reflects a fundamental difference between noble gases and network-bound species. Elements such as Li, Mg, Ca or Fe interact directly with the silicate structure, and their diffusivities are therefore closely linked to the degree of coupling with the network. In contrast, noble gases

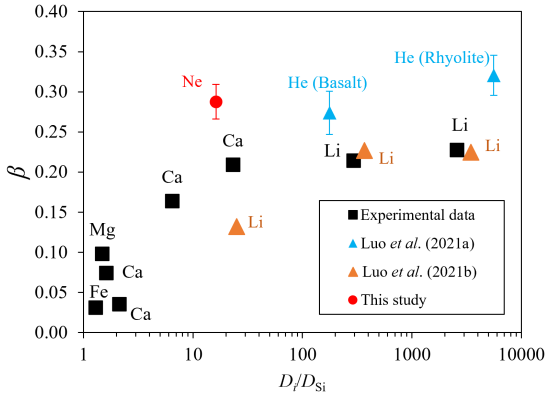

Figure 3 Relationship between the mass dependence exponent β and the solvent-normalised diffusivity (D_i/D_{Si}), modified from Luo *et al.* (2021a). Li and He data are from Luo *et al.* (2021a, 2021b); experimental data are from the references compiled therein.

diffuse through transient free volume regions generated by thermal fluctuations of the melt structure. Their absolute diffusivities are strongly influenced by atomic size, with He diffusing faster than Ne because it can more readily migrate through these transient pathways. However, once these pathways become accessible, the isotope dependence of diffusion appears to be governed by similar interactions with the dynamic silicate network, resulting in comparable β values for He and Ne. The noble gas data therefore suggest that the β-D_i/D_{Si} relationship established primarily from network-bound species may not be directly transferable to weakly interacting interstitial species. Additional experimental and computational studies on noble gas diffusion in silicate melts will be required to determine whether a distinct scaling relationship applies to this class of elements.

Discussion and Conclusions

The mass dependence of neon diffusion quantified in this study provides a physically grounded framework for evaluating diffusion-driven isotope fractionation during magmatic degassing. Across the investigated temperature range, the linear relationship between log D and log m confirms that isotopic mass exerts a measurable control on neon mobility in MORB melts (Fig. 2a). However, the derived mass dependence exponents (β = 0.24–0.29) remain substantially lower than the gas kinetic prediction of β = 0.5, reflecting the influence of the dense silicate network on atomic transport. These results demonstrate that melt-specific β values should be used when modelling noble gas isotope fractionation in magmatic systems.

The consequences of these reduced β values depend on the scale at which isotope fractionation is considered. At the bulk melt scale, the relatively low β values obtained here at ambient pressure indicate that diffusion alone is unlikely to generate large, system-wide $^{20}Ne/^{22}Ne$ offsets, particularly under conditions approaching quasi-equilibrium or progressive gas loss during ascent. Figure 4a illustrates the predicted evolution of the bulk melt composition during diffusion-controlled neon loss. Isotopic fractionation in the melt-averaged composition remains limited over most of the degassing range, and the magnitude of the predicted shift is systematically smaller when using the β values constrained in this study ($\beta \approx 0.3$) than when adopting the theoretical gas kinetic limit of β = 0.5. Even at high degrees of neon loss, the melt-averaged ratio $(^{20}Ne/^{22}Ne)/(^{20}Ne/^{22}Ne)_0$ remains close to unity (generally above ~0.9 for β = 0.3). These results suggest that, in slowly ascending or efficiently re-equilibrating magmas, the primary mantle neon signature is likely to be largely preserved in the residual melt.

The situation is different at the scale of individual vesicles, where diffusion can generate localised and transient isotopic heterogeneities under strongly non-equilibrium degassing conditions. To evaluate the magnitude of such effects, we considered an idealised spherical vesicle of fixed radius embedded within the melt and examined the transient isotopic evolution resulting solely from diffusion-driven transport, assuming that transfer across the melt-vesicle interface does not introduce additional isotope fractionation. This time-dependent vesicle model (Fig. 4b) demonstrates that the faster diffusion of ^{20}Ne relative to ^{22}Ne leads to a transient enrichment of the light isotope in the gas phase, with peak $^{20}Ne/^{22}Ne$ ratios that depend sensitively on β. For an initial magma $^{20}Ne/^{22}Ne$ ratio of 12.7, representative of an implanted solar wind component (see Moreira and Charnoz, 2016), the maximum vesicle ratio reaches approximately 13.0 for β = 0.3, compared to about 13.2 for β = 0.5. Although the fractionation predicted using the MD-derived β values is smaller than that obtained using the theoretical gas kinetic value β = 0.5, the resulting vesicle isotopic compositions remain comparable to the highest $^{20}Ne/^{22}Ne$ ratios reported for mantle-derived materials, which range from approximately 12.5 to 13.0 (Moreira and Charnoz, 2016). These results indicate that diffusion-driven fractionation is sufficiently large to generate measurable isotopic variations that may contribute to the neon isotope variability observed in natural magmatic systems, particularly if rapid ascent or quenching limits subsequent re-equilibration between the melt and the gas phase.

The pressure dependence of β further constrains the depth range over which diffusion-driven fractionation is expected to be most effective. The linear decrease of β with increasing pressure observed in our simulations implies that isotopic mass effects are progressively suppressed in deeper parts of ascending magmas. This is consistent with pressure-induced structural compaction of the melt, which enhances atomic coordination and promotes more collective transport mechanisms, thereby reducing the contribution of uncorrelated, mass-dependent diffusion. As a result, diffusion-controlled fractionation is expected to be weakest during early stages of ascent and bubble nucleation at high lithostatic pressures, and to become more effective only at shallower levels where degassing proceeds under stronger disequilibrium.

Taken together, these results demonstrate that the commonly assumed value of β = 0.5 is not appropriate for describing neon diffusion in silicate melts. Instead, a lower, melt-specific value of $\beta \approx 0.3$ at low pressure, with further reduction under compression, provides a more realistic and physically grounded basis for modelling isotope fractionation during magmatic degassing. While this implies that diffusion-driven fractionation is smaller than previously inferred from kinetic models, it remains sufficiently large to generate measurable, and potentially preserved, isotopic signatures in vesicles formed under

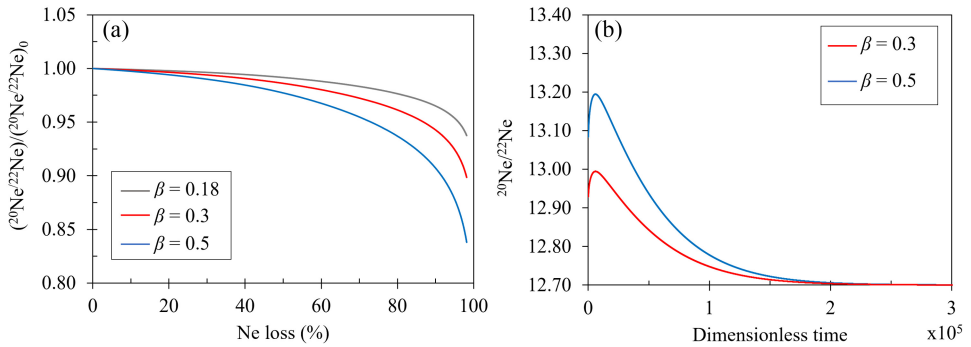

Figure 4 **(a)** Normalised melt $^{20}Ne/^{22}Ne$ as a function of neon loss for different β values. **(b)** Transient evolution of vesicle $^{20}Ne/^{22}Ne$ during diffusion-controlled degassing for β = 0.3 and 0.5, assuming 1 % vesicularity and an initial $^{20}Ne/^{22}Ne$ of 12.7.

rapid ascent or quenching conditions. Consequently, neon isotopic ratios measured in vesiculated volcanic glasses should not always be interpreted as direct proxies for mantle source compositions, but rather as records that may carry a superimposed, diffusion-controlled signature acquired during magma ascent and degassing.

Acknowledgments

The authors acknowledge support from the European Research Council (ERC) (Grant Agreement No. 101096688[APATE][ERC-2022-ADG]).

Editor: Horst R. Marschall

Additional Information

Supplementary Information accompanies this letter at https://www.geochemicalperspectivesletters.org/article2630.

Cite this letter as: Nteme, J., Moreira, M. (2026) Diffusional fractionation of neon isotopes in MORB melts: a molecular dynamics study. *Geochem. Persp. Let.* 41, 35–39. https://doi.org/10.7185/geochemlet.2630

References

Avice, G., Marty, B., Burgess, R. (2017) The origin and degassing history of the Earth's atmosphere revealed by Archean xenon. *Nature Communications* 8, 15455. https://doi.org/10.1038/ncomms15455

Ballentine, C.J., Marty, B., Sherwood Lollar, B., Cassidy, M. (2005) Neon isotopes constrain convection and volatile origin in the Earth's mantle. *Nature* 433, 33–38. https://doi.org/10.1038/nature03182.

Bekaert, D.V., Broadley, M.W., Caracausi, A., Marty, B. (2019) Novel insights into the degassing history of Earth's mantle from high precision noble gas analysis of magmatic gas. *Earth and Planetary Science Letters* 525, 115766. https://doi.org/10.1016/j.epsl.2019.115766

Goel, G., Zhang, L., Lacks, D.J., Van Orman, J.A. (2012) Isotope fractionation by diffusion in silicate melts: Insights from molecular dynamics simulations. *Geochimica et Cosmochimica Acta* 93, 205–213. https://doi.org/10.1016/j.gca.2012.07.008

Graham, T. (1833) XXVII. On the law of the diffusion of gases. *The London, Edinburgh, and Dublin Philosophical Magazine and Journal of Science* 2, 175–190. https://doi.org/10.1080/14786443308648004

Guillot, B., Sator, N. (2007) A computer simulation study of natural silicate melts. Part I: Low pressure properties. *Geochimica et Cosmochimica Acta* 71, 1249–1265. https://doi.org/10.1016/j.gca.2006.11.015

Honda, M., McDougall, I., Patterson, D.B., Doulgeris, A., Clague, D.A. (1993) Noble gases in submarine pillow basalt glasses from Loihi and Kilauea, Hawaii: a solar component in the Earth. *Geochimica et Cosmochimica Acta* 57, 859–874. https://doi.org/10.1016/0016-7037(93)90174-U

Kurz, M.D., Curtice, J., Fornari, D., Geist, D., Moreira, M. (2009) Primitive neon from the center of the Galápagos hotspot. *Earth and Planetary Science Letters* 286, 23–34. https://doi.org/10.1016/j.epsl.2009.06.008

Luo, H., Karki, B.B., Ghosh, D.B., Bao, H. (2020) First-principles computation of diffusional Mg isotope fractionation in silicate melts. *Geochimica et Cosmochimica Acta* 290, 27–40. https://doi.org/10.1016/j.gca.2020.08.028

Luo, H., Karki, B.B., Ghosh, D.B., Bao, H. (2021a) Diffusional fractionation of helium isotopes in silicate melts. *Geochemical Perspectives Letters* 19, 19–22. https://doi.org/10.7185/geochemlet.2128

Luo, H., Karki, B.B., Ghosh, D.B., Bao, H. (2021b) Deep neural network potentials for diffusional lithium isotope fractionation in silicate melts. *Geochimica et Cosmochimica Acta* 303, 38–50. https://doi.org/10.1016/j.gca.2021.03.031

Lux, G. (1987) The behavior of noble gases in silicate liquids: Solution, diffusion, bubbles and surface effects, with applications to natural samples. *Geochimica et Cosmochimica Acta* 51, 1549–1560. https://doi.org/10.1016/0016-7037(87)90336-X

Marty, B., Avice, G., Sano, Y., Altwegg, K., Balsiger, H., Hässig, M., *et al.* (2016) Origins of volatile elements (H, C, N, noble gases) on Earth and Mars in light of recent results from the ROSETTA cometary mission. *Earth and Planetary Science Letters* 441, 91–102. https://doi.org/10.1016/j.epsl.2016.02.031

Mizuno, H., Nakazawa, K., Hayashi, C. (1980) Dissolution of the primordial rare gases into the molten Earth's material. *Earth and Planetary Science Letters* 50, 202–210. https://doi.org/10.1016/0012-821X(80)90131-4

Moreira, M. (2013) Noble Gas Constraints on the Origin and Evolution of Earth's Volatiles. *Geochemical Perspectives* 2, 229–403. https://doi.org/10.7185/geochempersp.2.2

Moreira, M., Charnoz, S. (2016) The origin of the neon isotopes in chondrites and on Earth. *Earth and Planetary Science Letters* 433, 249–256. https://doi.org/10.1016/j.epsl.2015.11.002

Moreira, M., Staudacher, T., Sarda, P., Schilling, J.-G., Allègre, C.J. (1995) A primitive plume neon component in MORB: The Shona ridge-anomaly, South Atlantic (51–52°S). *Earth and Planetary Science Letters* 133, 367–377. https://doi.org/10.1016/0012-821X(95)00080-V

Moreira, M., Kunz, J., Allègre, C. (1998) Rare gas systematics in popping rock: isotopic and elemental compositions in the upper mantle. *Science* 279, 1178–1181. https://doi.org/10.1126/science.279.5354.1178

Moreira, M., Breddam, K., Curtice, J., Kurz, M.D. (2001) Solar neon in the Icelandic mantle: new evidence for an undegassed lower mantle. *Earth and Planetary Science Letters* 185, 15–23. https://doi.org/10.1016/S0012-821X(00)00351-4

Núñez-Guerrero, E., Moreira, M., Scaillet, B. (2025) Isotopic fractionation of neon during magma degassing. *Geochemical Perspectives Letters* 34, 1–5. https://doi.org/10.7185/geochemlet.2505

Ozima, M., Podosek, F.A. (1983) *Noble Gas Geochemistry*. First Edition, Cambridge University Press, Cambridge.

Péron, S., Moreira, M., Colin, A., Arbaret, L., Putlitz, B., Kurz, M.D. (2016) Neon isotopic composition of the mantle constrained by single vesicle analyses. *Earth and Planetary Science Letters* 449, 145–154. https://doi.org/10.1016/j.epsl.2016.05.052

Péron, S., Moreira, M., Putlitz, B., Kurz, M. (2017) Solar wind implantation supplied light volatiles during the first stage of Earth accretion. *Geochemical Perspectives Letters* 3, 151–159. https://doi.org/10.7185/geochemlet.1718

Péron, S., Moreira, M., Agranier, A. (2018) Origin of light noble gases (He, Ne, and Ar) on Earth: A review. *Geochemistry, Geophysics, Geosystems* 19, 979–996. https://doi.org/10.1002/2017GC007388

Péron, S., Mukhopadhyay, S., Kurz, M.D., Graham, D.W. (2021) Deep-mantle krypton reveals Earth's early accretion of carbonaceous matter. *Nature* 600, 462–467. https://doi.org/10.1038/s41586-021-04092-z

Sarda, P., Staudacher, T., Allègre, C.J. (1988) Neon isotopes in submarine basalts. *Earth and Planetary Science Letters* 91, 73–88. https://doi.org/10.1016/0012-821X(88)90152-5

Thompson, A.P., Aktulga, H.M., Berger, R., Bolintineanu, D.S., Brown, W.M., Crozier, P.S., *et al.* (2022) LAMMPS - a flexible simulation tool for particle-based materials modeling at the atomic, meso, and continuum scales. *Computer Physics Communications* 271, 108171. https://doi.org/10.1016/j.cpc.2021.108171

Trieloff, M., Kunz, J., Allègre, C.J. (2002) Noble gas systematics of the Réunion mantle plume source and the origin of primordial noble gases in Earth's mantle. *Earth and Planetary Science Letters* 200, 297–313. https://doi.org/10.1016/S0012-821X(02)00639-8

Watkins, J.M., DePaolo, D.J., Ryerson, F.J., Peterson, B.T. (2011) Influence of liquid structure on diffusive isotope separation in molten silicates and aqueous solutions. *Geochimica et Cosmochimica Acta* 75, 3103–3118. https://doi.org/10.1016/j.gca.2011.03.002

Yatsevich, I., Honda, M. (1997) Production of nucleogenic neon in the Earth from natural radioactive decay. *Journal of Geophysical Research: Solid Earth* 102, 10291–10298. https://doi.org/10.1029/97JB00395

Diffusional fractionation of neon isotopes in MORB melts: a molecular dynamics study

J. Nteme, M. Moreira

Supplementary Information

The Supplementary Information includes:

- Interaction Potentials and Parameters
- Numerical Modelling of Diffusion-Driven Neon Isotope Fractionation
- Tables S-1 to S-4
- Figures S-1 to S-3
- Supplementary Information References

Interaction Potentials and Parameters

The melt structure was modeled using the empirical potential developed for silicate melts of the KNCFMATS system (K_2O–Na_2O–CaO–FeO–MgO–Al_2O_3–TiO_2–SiO_2), first described by Guillot and Sator (2007) and later improved by Dufils *et al.* (2017). The interaction energy between atoms of the melt is given by a sum of pairwise contributions:

$$v(r_{ij}) = \frac{q_i\, q_j}{r_{ij}} + A_{ij}\ exp\left[-\left(\frac{r_{ij} - l_{ij}}{\lambda}\right)^2\right] + B_{ij}\ exp\left(-\frac{r_{ij}}{\rho_{ij}}\right) - \frac{C_{ij}}{r_{ij}^6}, \qquad \text{Eq. S-1}$$

where r_{ij} is the distance between atoms i and j, q_i is the effective charge of atom i. A_{ij}, l_{ij} and λ describe the covalent contribution, whereas B_{ij} and ρ_{ij} define the short-range repulsive interaction. The parameter C_{ij} corresponds to the dispersive (van der Waals) contribution. Neon atoms did not participate in any bonding interactions with the silicate network. Their interactions with the melt atoms (Si, O, Mg, Fe, etc.) were described using Lennard-Jones (LJ) potentials of the form:

$$v(r_{ij}) = 4\varepsilon\left[\left(\frac{\sigma}{r_{ij}}\right)^{12} - \left(\frac{\sigma}{r_{ij}}\right)^{6}\right] \qquad \text{Eq. S-2}$$

where ε is the depth of the Lennard–Jones potential well (i.e., the strength of the Ne–melt interaction), whereas σ is the finite-distance parameter at which the Lennard–Jones potential is zero and defines the effective size of the interacting atoms. These parameters are chosen to reproduce the weak, non-reactive nature of Ne–melt interactions, consistent with previous studies on noble gas solubility in silicate melts (Carroll and Stolper, 1993). All interaction parameters used in this study are reported in the following Tables S-1 and S-2.

Table S-1 Potential parameters for silicates (Dufils *et al.*, 2017). Values of *A*, *l, B*, *ρ* and *C* given in columns 3, 4, 5, 6, and 7, respectively, correspond to oxygen-oxygen and cation-oxygen interactions. The cation-cation interactions are described only by repulsive Coulomb forces. Note that there is no covalent interaction energy between oxygen atoms. The parameter λ in the cation-oxygen covalent energy is equal to 0.1414 Å.

	qi (e)	A (kJ/mol)	l (Å)	B (kJ/mol)	ρ (Å)	C (Å6 kJ/mol)
O	-0.945	0	0	153000	0.325	5259.83
Si	1.85	50	1.61	4869260	0.157	3036.49
Ti	1.85	32.2	1.9	5372350	0.182	9181.15
Al	1.4175	39.3	1.75	2681580	0.17	2564.84
Fe^{3+}	1.4175	40.65	1.85	1761660	0.196	7034.76
Fe^{2+}	0.945	30.2	2.05	2193830	0.194	6428.64
Mg	0.945	28.4	2	3275780	0.18	3912.7
Ca	0.945	18.6	2.4	15640400	0.179	8271.3
Na	0.4725	7.8	2.47	11937700	0.173	4673.81
K	0.4725	5.65	2.9	941307	0.242	8653.71

Table S-2 Lennard–Jones potential parameters for Ne–silicate interactions (Guillot and Sator, 2012).

	ε (kJ/mol)	σ (Å)
O	0.691	2.814
Si	7.82	1.747
Ti	8.937	2.038
Al	4.206	1.873
Fe3+	8.325	1.97
Fe2+	4.113	2.173
Mg	2.896	2.125
Ca	2.142	2.513
Na	0.984	2.6
K	0.663	3.056

Numerical Modelling of Diffusion-Driven Neon Isotope Fractionation

The diffusion coefficients obtained from the molecular dynamics simulations were subsequently used in two independent numerical calculations designed to evaluate the consequences of diffusion-driven isotope fractionation at different scales. The first calculation examines the evolution of the average isotopic composition of the melt during diffusive neon loss. The second calculation investigates the transient isotopic evolution of an individual vesicle during disequilibrium degassing. These calculations address different questions and should be viewed as complementary sensitivity analyses rather than as components of a single degassing model.

Fractionation at the melt scale

This model describes isotope fractionation associated with diffusive neon loss from the melt as a whole, treating degassing as a spatially continuous transport process toward a melt–vesicle boundary. The evolution of neon concentration in the melt is governed by the one-dimensional diffusion equation

$$\frac{\delta C}{\delta t} = D\frac{\delta^2 C}{\delta x^2} \qquad \text{Eq. S-3}$$

with an initially homogeneous concentration field, a zero-flux boundary condition at the melt interior, and a sink condition imposed at the degassing interface to represent the rapid and effectively irreversible transfer of neon into the vapor phase. The dependence of diffusivity on isotopic mass is introduced through the scaling $D(m) = D_{ref}\left(m/m_{ref}\right)^{-\beta}$, where m_{ref} = 20 g/mol and D_{ref} is the diffusion coefficient of ^{20}Ne. The governing equation is solved using a Crank–Nicolson finite-difference scheme. Spatial integration of the concentration profiles yields the cumulative fractional losses of ^{20}Ne and ^{22}Ne and the evolution of the melt-averaged normalized isotopic ratio $(^{20}Ne/^{22}Ne)/(^{20}Ne/^{22}Ne)_0$ as a function of total neon loss.

Fractionation within the vesicle

This second model focuses on the local, transient isotope fractionation that develops within an individual vesicle during disequilibrium degassing. The vesicle–melt system is represented by a spherically symmetric radial domain, consisting of a vesicle of radius a surrounded by a melt shell extending to an outer radius R. The geometry is assumed to remain constant throughout the calculation, providing a simplified framework in which the diffusion-driven component of isotope fractionation can be isolated. The model is therefore intended to evaluate the transient isotopic response of a local gas reservoir rather than to reproduce the complete evolution of a growing vesicle during magma degassing.

Neon transport in the melt is described by Fick's second law and solved numerically using an explicit finite-difference scheme. At the vesicle–melt interface, a sink boundary condition is imposed to account for the rapid and effectively irreversible transfer of neon into the vesicle, whereas a zero-flux boundary condition is applied at the outer edge of the melt domain. This formulation assumes that transfer across the melt–vesicle interface does not introduce any additional isotope fractionation, so that the overall isotopic selectivity is controlled solely by the diffusion coefficients of neon isotopes in the melt. Separate simulations are performed for ^{20}Ne and ^{22}Ne, and the vesicle-integrated neon inventories are tracked through time to calculate the transient evolution of the isotopic ratio ($^{20}Ne/^{22}Ne$) within the vesicle. The numerical solution yields isotope fractionation as a function of a dimensionless time variable, which can be subsequently rescaled using a characteristic diffusion time $\tau = (R - a)^2/D_{ref}$, where a is the vesicle radius, R is the outer radius of the melt domain, and D_{ref} is the diffusion coefficient of ^{20}Ne in the basaltic melt (7.7×10^{-10} m^2 s^{-1} at 1473 K).

The numerical implementations corresponding to these two models are provided in separate code files.

Supplementary Tables

Table S-3 Chemical composition (wt %) of the silicate (MORB) melt investigated in this study. Data are from Reynolds and Langmuir (1997). In parentheses are the numbers of cations of each species used in the simulation. The overall charge neutrality of the system is ensured by the appropriate number of oxygen atoms.

Oxides	wt %
SiO_2	50.59 (555)
TiO_2	1.52 (12)
Al_2O_3	15.11 (195)
Fe_2O_3	1.15 (9)
FeO	8.39 (78)
MgO	7.77 (126)
CaO	11.87 (141)
Na_2O	2.94 (63)
K_2O	0.13 (3)
Total	99.47

Table S-4 Diffusion coefficients of Ne pseudo-isotopes in the studied basalt melt at different temperatures and pressures.

T (K)	P (kbar)	m_{Ne} (g/mol)	D_{Ne} (10^{-9} m²/s)
1473	0	4	1.11 ± 0.05
1473	0	8	1.01 ± 0.04
1473	0	12	0.90 ± 0.04
1473	0	16	0.79 ± 0.03
1473	0	20	0.77 ± 0.04
1673	0	4	2.57 ± 0.07
1673	0	8	2.19 ± 0.07
1673	0	12	1.91 ± 0.04
1673	0	16	1.73 ± 0.05
1673	0	20	1.62 ± 0.05
1873	0	4	4.74 ± 0.11
1873	0	8	3.98 ± 0.09
1873	0	12	3.60 ± 0.08
1873	0	16	3.24 ± 0.09
1873	0	20	3.04 ± 0.07
1873	5	4	3.62 ± 0.07
1873	5	8	3.00 ± 0.05

Table S-4 continued.

T (K)	P (kbar)	m_{Ne} (g/mol)	D_{Ne} (10^{-9} m²/s)
1873	5	12	2.78 ± 0.08
1873	5	16	2.62 ± 0.05
1873	5	20	2.56 ± 0.08
1873	10	4	2.84 ± 0.05
1873	10	8	2.52 ± 0.05
1873	10	12	2.30 ± 0.05
1873	10	16	2.28 ± 0.05
1873	10	20	2.08 ± 0.07

Supplementary Figures

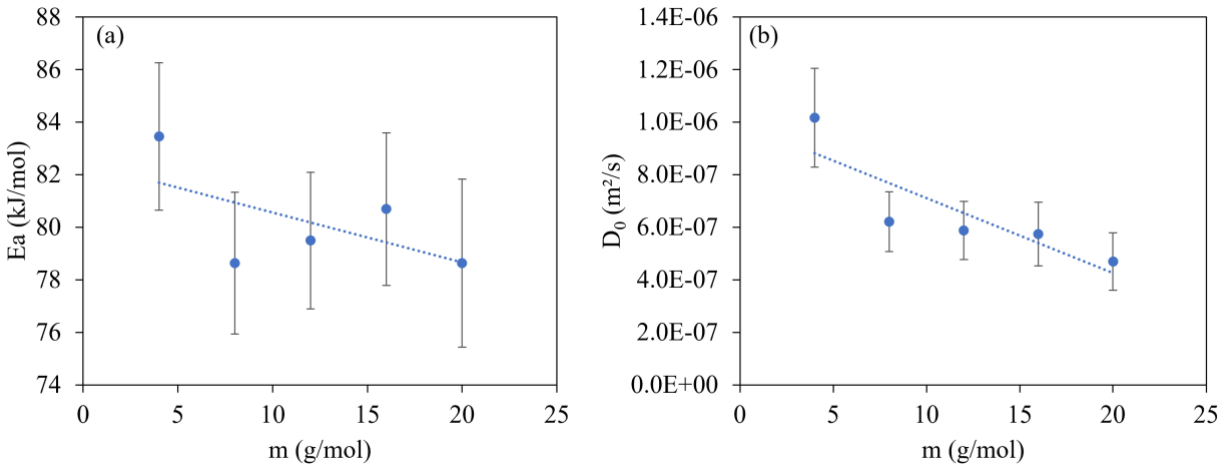

Figure S-1 Activation energy (E_a) and predicted pre-exponential factor (D_0) for Ne isotopes as a function of isotopic mass in the investigated basalt melt.

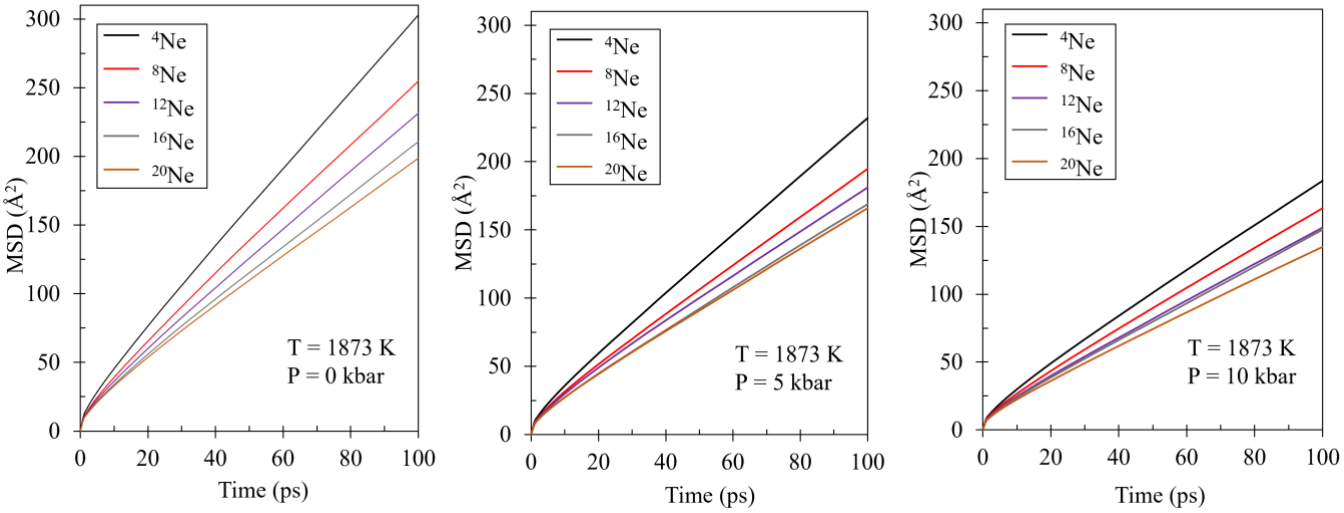

Figure S-2 Mean squared displacement (MSD) of Ne pseudo-isotopes at 1873 K under pressures of 0, 5, and 10 kbar.

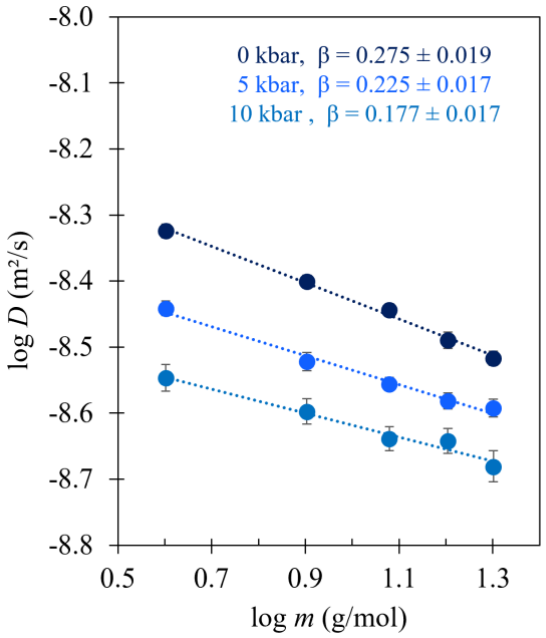

Figure S-3 Log–log plot of the diffusion coefficients of Ne pseudo-isotopes in the studied basaltic melt at 1873 K under pressures of 0, 5, and 10 kbar.

Supplementary Information References

Carroll, M.R., Stolper, E.M. (1993) Noble gas solubilities in silicate melts and glasses: New experimental results for argon and the relationship between solubility and ionic porosity. *Geochimica et Cosmochimica Acta* 57, 5039–5051. https://doi.org/10.1016/0016-7037(93)90606-W

Dufils, T., Folliet, N., Mantisi, B., Sator, N., Guillot, B. (2017) Properties of magmatic liquids by molecular dynamics simulation: the example of a MORB melt. *Chemical Geology* 461, 34–46. https://doi.org/10.1016/j.chemgeo.2016.06.030

Guillot, B., Sator, N. (2007) A computer simulation study of natural silicate melts. Part I: Low pressure properties. *Geochimica et Cosmochimica Acta* 71, 1249–1265. https://doi.org/10.1016/j.gca.2006.11.015

Guillot, B., Sator, N. (2012) Noble gases in high-pressure silicate liquids: A computer simulation study. *Geochimica et Cosmochimica Acta* 80, 51–69. https://doi.org/10.1016/j.gca.2011.11.040

Reynolds, J.R., Langmuir, C.H. (1997) Petrological systematics of the Mid-Atlantic Ridge south of Kane: Implications for ocean crust formation. *Journal of Geophysical Research: Solid Earth* 102, 14915–14946. https://doi.org/10.1029/97JB00391